Thin Solid Films 573 (2014) 191–195

Contents lists available at ScienceDirect

Thin Solid Films

journal homepage: www.elsevier.com/locate/tsf

Quantum-confined photoluminescence from size-controlled boron doped nanocrystalline-Si:H/a-SiC$_x$:H superlattice

Jun Ma, Jian Ni *, JianJun Zhang, Qun Liu, XiaoDan Zhang, Ying Zhao

Institute of Photo-electronics Thin Film Devices and Technique of Nankai University, Tianjin 300071, China
Key Laboratory of Photo-electronics Thin Film Devices and Technique of Tianjin, Tianjin 300071, China
Key Laboratory of Photo-Electronic Information Science and Technology of Ministry of Education, Nankai University, Tianjin 300071, China

ARTICLE INFO

Article history:
Received 7 April 2014
Received in revised form 12 November 2014
Accepted 12 November 2014
Available online 20 November 2014

Keywords:
Quantum dot superlattices
Quantum confinement effect
Optoelectronics
Plasma-enhanced chemical vapor deposition

ABSTRACT

Boron doped nanocrystalline-Si:H/a-SiC$_x$:H (nc-Si:H/a-SiC$_x$:H) quantum dot superlattice has been prepared by plasma enhanced chemical vapor deposition at a low temperature of 150 °C. This method for fabricating superlattice allows controlling both the size and density of Si quantum dots in potential well and the characteristics of potential barrier without subsequent annealing treatment. Cross-section high resolution transmission electron microscopy investigations confirm the periodic multi-layer structure of silicon quantum dots (~2 nm diameter) separated by a-SiC$_x$:H matrix (2–3 nm thickness) with sharp interface. With strong blue photoluminescence and high perpendicular conductivity, boron doped nc-Si:H/a-SiC$_x$:H quantum dot superlattice shows great advantages in obtaining applicable blue light emission.

1. Introduction

Since the visible photoluminescence (PL) of porous silicon at room temperature was firstly reported by Canham [1], the incorporation of silicon-based nanostructures [2,3] has been one of the major advances in optoelectronics and photonic circuits. Considerable interest has been drawn toward its attractive properties such as quantum-confined photoluminescence and good band gap engineering to obtain a tunable light-emission. However, it has been reported that the PL peak energy of porous silicon does not increase beyond 2.1 eV even when the crystallite size drops well below 3 nm [4,5]. In addition, efficient PL has been observed in silicon quantum dot superlattices (QDSLs), in which the silicon nanocrystal layer is fabricated ultra-thin in one dimension and separated by potential barrier to increase its effective band gap [6,7]. So far, researchers devoted their great efforts to nc-Si:H/SiC materials which have shown exciting prospects for emitting short-wavelength visible light [8,9]. As compared to the porous silicon, relatively high PL peak energy could be achieved in nc-Si:H/SiC materials due to the strain elimination and better passivation of Si–C bonds at well/barrier interface. Considering the advantages of SiC itself such as stability and flexibility, nc-Si:H/SiC QDSL approach was of great potential for application in photoelectric devices.

Unfortunately, little has been reported on the strong PL spectra of Si quantum dots (QDs) embedded in SiC matrix fabricated by high temperature (~1000 °C) post-annealing processing [10,11]. For one reason the potential well and barrier in the real material may be irregular at the interface, which decreases the electronic states and associated confinement effects consequently. Moreover, SiC and Si materials possess similar covalent electron structure, which brings about the segregation and precipitation effect for Si in SiC matrix. Besides strong blue PL spectra, the conductivity of QDSL material also plays an important role in the enhancement of the carrier injection, which improves the luminescent properties and the carrier collection efficiency in light emitting devices. However, serious problems exist in utilizing boron doped Si QDSLs in reality, especially for the ones prepared through phase separation of sub-stoichiometric layers in high temperature post-annealing processing. It has been reported that the formation energy of dopant addition to Si nanocrystals is higher than that of bulk Si. Because of this, it is not clear at present whether or not the doping of Si QDs provides the generation of free charge carriers [12,13].

It has been reported recently that room-temperature photoluminescence was observed in p-nc-Si:H/a-SiC$_x$:H quantum dot superlattice [14]. In this paper, boron doped nc-Si:H/a-SiC$_x$:H QDSLs were successfully fabricated by plasma enhanced chemical vapor deposition (PECVD) at a low temperature of 150 °C without subsequent annealing treatment. Strong PL in the blue-green range and peak energy shift was observed at room temperature, indicative of quantum confinement effects. With short PL decay time (below 3.0 ns) and high perpendicular conductivity, boron doped nc-Si:H/a-SiC$_x$:H QDSLs were of great

* Corresponding author at: Institute of Photo-electronics Thin Film Devices and Technique of Nankai University, Tianjin 300071, China.
E-mail address: elsevier_jianni@163.com (J. Ni).

http://dx.doi.org/10.1016/j.tsf.2014.11.041
0040-6090/

potential for application in ultraviolet-light detectors and other optoelectronic devices.

2. Experimental details

Boron doped nc-Si:H/a-SiC_x:H QDSLs were prepared by the layer by layer growth scheme in plasma-enhanced chemical vapor deposition system. In this work, the alternating process comprises the depositions of 3 nm a-SiC_x:H barrier layer, 4 nm p-nc-Si:H well layer and subsequent H plasma treatments in 3 periods (Fig. 1). The a-SiC_x:H layer was deposited from appropriated gaseous mixture of SiH_4, CH_4 and H_2 at 'low-power regime' [15]. Hydrogen plasma treatments were attained to etch the amorphous portion and consequently promote sharp interface on the surface of p-nc-Si:H, which facilitates the direct surface passivation of Si nanocrystals by Si–C bonds. The Si nanocrystals of p-nc-Si:H layer were well size-controlled by varying the silane concentrations ($[SiH_4]\% = SiH_4 / (SiH_4 + H_2)\%$) in the reaction precursor. Specially, different samples labeled as A, B and C were fabricated with a decreased $[SiH_4]$% of 1%, 0.6% and 0.3% respectively. Moreover, in order to investigate the influence of the barrier height on the properties of p-nc-Si:H/a-SiC_x:H films, CH_4 concentrations ($[CH_4]\% = CH_4 / (CH_4 + SiH_4)\%$) were also adjusted as 65% for samples A, B and C while increased to 70% and 75% corresponding to samples D and E respectively. The total thickness of each thin-film was made to be approximately 20 nm. The electrode distance was kept as 25 mm. The detailed deposition parameters of QDSL samples were presented in Table 1.

The structural characteristics of the samples were studied by glancing incidence X-ray diffraction (GIXRD) (Rigaku D/max 2500v/pc) operating with CuKα radiation. The glancing angle between the incident X-ray beam and the sample surface was set as 0.26°, close to the critical angle. The Raman spectroscopy was performed using a He–Cd laser with a wavelength of 325 nm. The structural characteristics of p-nc-Si:H/a-SiC_x:H QDSLs were investigated by plane view and cross section transmission electron microscopy (TEM) in Philips Tecnai G^2F20 electron microscopes with 2000 kV operating voltage. Room temperature PL spectra and PL decay time measurement were carried out by the Rapid Photoluminescence Mapper RPM2000 with 325 nm excitation. The perpendicular transport behavior of samples was investigated through a sandwich structure with an Al electrode on top of the samples and the other on the substrates of stainless steel. In addition, different a-SiC_x:H films were respectively deposited on Corning 7059 substrates. Reflectance and transmittance (RT) measurements were performed at normal incidence in the spectral range between 200 and 1800 nm with a double beam Cary 5000 spectrophotometer. The optical band gap of thin a-SiC_x:H film was calculated with the following equation

$$(\alpha h\nu)^{1/2} = B\left(h\nu - E_g\right),$$

where α is the absorption coefficient, h is the Planck's constant, ν is the photo frequency, B is the proportionality constants, and E_g is the optical band gap. The perpendicular transport behavior of materials was investigated through a sandwich structure with an Al electrode on top of the samples and the other electrode on the substrates, the current flow is perpendicular to the substrate. The measuring errors to the conductivity values are about ±0.1%.

Table 1
Deposition conditions of different QDSL samples.

Process	T_s (°C)	SiH_4 flow (sccm)	CH_4 flow (sccm)	B_2H_6 flow (sccm)	H_2 flow (sccm)	Pressure (Torr)	Power (W)	Time (m)
A: p-nc-Si:H	150	6	0	6	59	2	250	1
A: a-SiC_x:H	150	5	0.9	0	60	0.6	12	3
B: p-nc-Si:H	150	6	0	6	100	2	250	1.5
B: a-SiC_x:H	150	5	0.9	0	60	0.6	12	3
C: p-nc-Si:H	150	6	0	6	200	2	250	2
C: a-SiC_x:H	150	5	0.9	0	60	0.6	12	3
D: p-nc-Si:H	150	6	0	6	59	2	250	1
D: a-SiC_x:H	150	5	1.2	0	60	0.6	12	3
E: p-nc-Si:H	150	6	0	6	59	2	250	1
E: a-SiC_x:H	150	5	1.5	0	60	0.6	12	3
Hydrogen treatment	150	0	0	0	50	1	20	0.5

3. Results and discussion

As illustrated in Fig. 2, the structural information of the samples was firstly investigated by GIXRD. Two main peaks are evident in all samples, which are attributed to the Bragg peaks of Si (111) and (220), indicating the formation of nanocrystalline Si. The diffraction angle (~28.4°, ~47.4°) gradually increased as $[SiH_4]$% decreases from 1% to 0.3%. Combined with the emergence of the Bragg peaks of Si (311), it could be concluded that a larger size of nanocrystalline Si and crystalline volume fraction might be achieved in samples B and C. Furthermore, Raman measurements and Gaussian deconvolution were carried out (Fig. 3). All samples exhibit two peaks at 480 cm^{-1} and ~520 cm^{-1}, representing the contributions of both amorphous and crystalline phases. According to the confinement model [16], the mean size of silicon nanocrystals in the mix-phase films can be calculated as ~2 nm, ~2.5 nm and ~3 nm for samples A, B and C, respectively. Associated with the decrease of $[SiH_4]$%, plenty of H atoms in the plasma were expected to etch the dangling bond on the surface, which in turn facilitates the mobility of reaction precursor as well as the relaxation of Si network.

Since XRD and Raman measurements cannot provide unambiguous information regarding the size and the dislocation density of quantum dots, additional structural information of p-nc-Si:H/a-SiC_x:H QDSLs was obtained by the high-resolution TEM image in Fig. 4. The phase separation and meticulous superlattice structure are clearly identified with relatively sharp interface by cross-section TEM images (Fig. 4(a)). The nanocrystalline Si of ~2 nm in the p-nc-Si:H quantum wells is embraced by a-SiC_x:H matrix at interface with gains connecting with each other, which is in an agreement with Raman results. According to the Bragg's Law and Ewald Method, the radii and ratio patterns of crystallographic rings are deduced from transmission electron diffractogram (TED, Fig. 4(b)) and lead to the visualization of two main planes of the Si

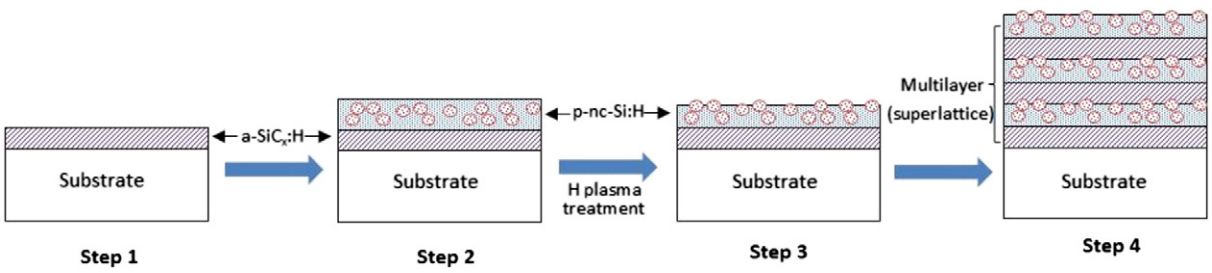

Fig. 1. The detailed deposition process of p-nc-Si:H/a-SiC_x:H QDSL samples (1) a single a-SiC_x:H layer and (2) p-nc-Si:H layer, (3) H plasma treatments, and (4) a multilayer structure.